ELSEVIER

www.elsevier.nl/locate/jorganchem

Journal of Organometallic Chemistry 595 (2000) 248–260

Journal of Organometallic Chemistry

Matrix isolation infrared and density functional theoretical studies of cryogenic reactions of silicon atoms with dimethyl ether and methanol: new route to generation and stabilization of transient silanones

Valery N. Khabashesku *, Konstantin N. Kudin, John L. Margrave, Leif Fredin [1]

Department of Chemistry, Rice University, Houston, Houston, TX 77005-1892, USA

Accepted 4 October 1999

Abstract

Silicon atoms, produced by vaporization of silicon at temperatures 1450–1650°C from a graphite cell, were co-condensed with dimethyl ether or methanol and a large excess of argon onto a polished copper substrate cooled down to 15 K. The deposited solid matrixes were studied by reflection-transmission IR spectroscopy. Structural identification of the reactive intermediates, formed during co-condensation and subsequent photoirradiation of the primary products, and vibrational analysis of their spectra have been accomplished by comparison with the previously reported IR features for silylene CH_3OSiCH_3 (**2**) (G. Maier, H.P. Reisenauer, K. Schöttler, U. Wessolek-Kraus, J. Organomet. Chem. 366 (1989) 25), silanones $(CH_3)_2Si{=}O$ (**3**) (V.N. Khabashesku, Z.A. Kerzina, A.K. Maltsev, O.M. Nefedov, J. Organomet. Chem. 347 (1988) 277) and $CH_3(H)Si{=}O$ (**9**) (R. Withnall, L. Andrews, J. Am. Chem. Soc. 108 (1986) 8118), and with the density functional theory B3LYP/6-311G(d,p) calculated harmonic frequencies and infrared intensities for complexes $Si{\cdots}O(CH_3)_2$ (**1**) and $Si{\cdots}O(CH_3)H$ (**7**), silylenes (**2**), CH_3OSiH (**6**), CH_3SiOH (**8**), silanones (**3**) and (**9**), and 1-methyl-2-oxa-1-silirane (**4**) and oxasilirane (**10**). The step-wise mechanisms for the formation of the products **1**–**10** were suggested with the help of theoretical modeling based on DFT calculations of reaction dynamics of $Si(^1D)$ atoms with CH_3OCH_3 and CH_3OH. The directly observed formation of silanones (**3**) and (**9**) in the detectable by a standard IR spectrometer quantities suggests that the studied reactions can be utilized as a new route for generation and physical stabilization of transient silanones.

Keywords: Silanones; Silicon atoms; Cryogenic reactions; Matrix isolation; Infrared spectroscopy; Density functional calculations

1. Introduction

There has been an enhanced interest over the last decades in the studies of the surface chemistry of silicon, as well as of other semiconductors. The understanding and control of the chemistry involved in surface etching, doping, functionalization, and thin-film deposition is critical for the design and production of small electronic devices. The related reactions also play an important role in the industrial processes of direct synthesis of silanes. The chemical processes, proceeding on silicon surfaces during adsorption of various small inorganic and organic molecules, and elements, have been recently reviewed [1]. At the same time, in order to get a better insight into the mechanisms of surface reactions through learning about the reactive intermediates involved, the experimental and theoretical modeling of these reactions at atom–molecular level is particularly helpful [2]. Matrix isolation spectroscopy combined with quantum-chemical calculations provides an efficient modeling tool for this purpose.

The previous matrix isolation studies have encompassed the co-condensation reactions of silicon and germanium atoms with small inorganic molecules, such as H_2O, HF, H_2, and carbon in solid argon [3–8]. It was found that the reactions proceed either spontaneously or require photoexcitation (as in the case of H_2O) and result in metal atom insertion into O–H, H–F

* Corresponding author.

[1] Present address: Systems and Processing Engineering Corp., Austin, TX 78746-6558, USA.

0022-328X/00/$ - see front matter
PII: S0022-328X(99)00632-4

and H–H bonds with the formation of transient silylenes and germylenes, HSiOH [3,4], HGeOH [3], HSiF [5], SiH_2 [7], GeH_2 [8], and Si_2C species [6], respectively. The intermediate products, formed in the reactions of silicon atoms with HCN and N_2 in inert matrixes, have been examined recently by IR spectroscopy [9]. Theoretical studies on the reaction dynamics of these systems have so far involved the ab initio calculations of potential-energy surfaces for the interactions of ground and excited state silicon atoms with water, which predict that the formation of a $Si\cdots OH_2$ complex proceeds without a barrier [10].

The studies of cryogenic reactions of silicon atoms with organic molecules in inert matrixes are limited as well. The preliminary matrix isolation data [11,12] indicate that silicon atoms both in their ground and excited states do not react with methane. This agrees with the calculations of Gordon and co-workers [13], predicting a significant barrier (14 kcal mol^{-1} at the MP4 level of the theory) for the insertion of excited state $Si(^1D)$ atoms into the C–H bond in methane, while no transition state was found for the ground state $Si(^3P) + CH_4$ reaction. In the course of FTIR studies of the co-condensates of Si and Ge atoms with ethylene oxide in argon matrices at 12–15 K, new bands have been observed and assigned to the products of spontaneous metal atom insertion into the C–O bond in the strained ring. The four-member cyclic oxasilylene and oxagermylene structures of these products were suggested after comparison with the calculated spectra [12,14]. It has been reported recently [9] that the co-condensation reactions of silicon atoms with acetylene and ethylene in argon matrixes yield silacyclopropenylidene and silacyclopropylidene, respectively, as a primary products.

In the present paper we report matrix isolation infrared data on the reactions of Si atoms with CH_3OCH_3 and CH_3OH, and their interpretation based on density functional calculations of reaction dynamics, energies and vibrational spectra of reactive intermediates. For comparison purposes, the calculations were also carried out for the similar Ge atom reactions.

2. Experiment and calculations

2.1. Matrix isolation infrared spectroscopy

Silicon atoms were co-condensed with the selected reactant and a large excess of argon (1:500–1000) on a side surface of a polished copper block cooled to 12–15 K by an Air Products Displex CSW-202 closed-cycle helium refrigerator. The silicon was vaporized from a high-density graphite cell, heated resistively to temperatures from 1450 to 1650°C. The temperature of the cell was measured with an optical pyrometer. Deposition times were normally of the order of 1 h. The deposition rates and silicon/reactant/argon ratios were measured directly with a cooled quartz crystal microbalance mounted on one of the four sides of copper block

Matrices were irradiated either during or subsequent to deposition. The irradiation source used was a 100 W medium pressure mercury lamp which was focused to a 2 cm diameter spot on the matrix surface.

Silicon ($>99\%$) was obtained from MCB and used in these experiments without further purification. Dimethyl ether (99%) was purchased from MG Industries; methanol (99.9%) was acquired from Aldrich Chemical. Matheson argon (99.99%) was additionally purified by passing it through hot tantalum (900°C) prior to deposition.

The reflection–transmission IR spectra of deposited matrices were recorded on a Beckman IR-9 spectrometer. Frequencies were measured with an accuracy of ± 0.5 cm^{-1}. More detailed descriptions of the matrix isolation apparatus and spectrometer were given earlier [3–7].

2.2. Calculation procedures

All calculations have been performed with the GAUSSIAN 94 program [15] running on the NEC SX-3 supercomputer. The ground-state optimized geometries of the studied reaction products were computed at the density functional B3LYP level of theory [16,17] with the 6-311G(d,p) basis set of triple-zeta quality [18]. The harmonic vibrational frequencies were calculated from the analytic second derivatives of the energy available with the B3LYP method. The vibrational analysis of the computed frequencies was carried out with the help of XMOL vibration visualization program [19]. These data are given in Tables 1–10.

The transition-state energies were calculated to model the reactions of the Si and Ge atoms, considered to be in their excited ^1D states under the conditions of simultaneous deposition and photoirradiation of their co-condensates with dimethyl ether and methanol. For the search of the reaction transition states, a procedure, similar to that detailed in our previous paper [20], has been applied. The calculated absolute and zero-point vibrational energies for the ground and transition states, participating in the reactions studied, are summarized in the Table 11.

3. Results

3.1. IR spectra of the products of the reaction of Si with CH_3OCH_3

In the IR spectrum of argon matrix-isolated co-condensates of Si atoms with dimethyl ether, deposited at a substrate temperature of 15 K, besides the bands of

CH_3OCH_3 (Fig. 1(a)), a set of new bands at 869, 1042, 1143, 1456 and 1466 cm^{-1}, marked in Fig. 1(b) with filled circles, has been observed. The intensities of these new peaks have repeated those in the spectrum of matrix-isolated dimethyl ether (Fig. 1(a)). However, they were all shifted from the original CH_3OCH_3 peak locations to the lower wavenumbers (Fig. 1(b)), in agreement with the B3LYP predicted shifts.

This observation suggests strongly the formation of an $Si\cdots O(CH_3)_2$ complex (**1**) during co-condensation (Scheme 1), similar to the earlier detected $Si\cdots OH_2$ complex [5], and in agreement with the calculated spectrum of **1** (Table 1).

Table 1
Vibrational frequencies for complex $(CH_3)_2O\cdots Si$ (**1**)

Symmetry	Frequencies (cm^{-1})		Assignment
	Calculated [a]	Observed	
b_1	119(0.7) [b]		CH_3 torsion, i.p. [c]
a_2	168(0)		CH_3 torsion, o.p. [c]
b_1	263(4)		COC wag
b_2	271(0.1)		COC in-plane rock
a_1	279(19)		Si···O str.
a_1	444(30)		COC scissor
a_1	856(104)	869 s	C–O symmetry str.
b_2	1007(41)	1042 m	C–O asymmetry str.
a_2	1151(0)		CH_3 rock, i.p. [c]
b_2	1162(56)	1143 m	CH_3 in-plane rock, i.p. [c]
b_1	1184(8)		CH_3 symmetry out-of-plane rock
a_1	1255(1)		CH_3 symmetry in-plane rock
b_2	1429(21)	1456 w	CH_3 deformation, i.p. [c]
a_1	1458(0)		CH_3 deformation, o.p. [c]
b_2	1479(23)	1466 w	CH_3 asymmetry deformation
a_2	1484(0)		CH_3 asymmetry deformation
b_1	1501(15)		CH_3 symmetry deformation
a_1	1503(0.4)		CH_3 symmetry deformation
b_2	3017(37)		CH_3 asymmetry symmetry str.
a_1	3026(92)		CH_3 symmetry symmetry str.
b_1	3099(55)		CH_3 asymmetry str., i.p. [c]
a_2	3100(0)		CH_3 asymmetry str., o.p. [c]
b_2	3167(0.1)		CH_3 in-plane asymmetry str.
a_1	3172(2)		CH_3 in-plane symmetry str.

[a] B3LYP/6-311G(d,p).
[b] Calculated infrared intensities in km mol^{-1}.
[c] i.p., in phase; o.p., out of phase.

The subsequent irradiation of this matrix with unfiltered light from a mercury lamp ($\lambda > 200$ nm) led to a complete disappearance of the bands attributed to a complex **1** and the appearance of a series of new bands in the spectrum shown on Fig. 1(c). The bands, marked by their wavenumbers on this spectrum, match very well the most intense bands in the known spectrum of matrix-isolated dimethylsilanone (**3**) [21–23]. These bands have all disappeared during matrix warm-up to 35–40 K, along with the appearance of recognized cyclosiloxane absorption in the 1020–1080 cm^{-1} region [21–23]. The experimental and calculated vibrational frequencies and infrared intensities of **3** are given in Table 2.

Besides the bands of silanone (**3**), weaker bands, denoted by filled squares and empty circles on Fig. 1(c), were observed. The former bands coincide with the IR absorptions of methyl(methoxy)silylene (**2**) (as indicated in Table 3), detected earlier by Maier et al. [24] after the gas-phase thermal generation and subsequent trapping of this intermediate in the matrix. The latter bands (among which was a peak at 2110 cm^{-1}, located in the sp^3 Si–H stretch region) were assigned tentatively to 1-methyl-2-oxa-1-silirane (**4**) on the basis of mechanistic consideration (Scheme 1) and calculations of the energy profile of the reaction (Fig. 2), and are in reasonable agreement with the calculated vibrational spectrum of **4** (Table 4).

When the irradiation was used simultaneously with the co-deposition of Si, argon, and CH_3OCH_3 into a matrix, the IR spectrum of the resulting reaction products exhibited only the bands of silanone (**3**), which is the most likely to be photostable among the products **1**–**4**.

It should be noted that the bands of the other possible structural isomer of **2** — 1-methoxy-1-silene, $CH_3O(H)Si{=}CH_2$ (**5**), given in Table 5, were not detected in our experiments. According to Maier et al. [24], the isomerization of silylene (**2**) (which absorbs in the UV spectrum at 357 nm) into silene (**5**) (found to absorb at 245 nm) proceeds during irradiation of **2** with the filtered light ($\lambda > 310$ nm).

3.2. IR spectra of the products of the reaction of Si with CH_3OH

In the IR spectrum (Fig. 3(b)) of an argon matrix, produced by co-condensation of Si atoms with CH_3OH, we observed strong bands of methoxysilylene CH_3OSiH (**6**), the insertion product of silicon into the O–H bond of methanol (Scheme 2), already in the absence of photoactivation. The assignment to **6** of the bands, denoted by filled squares in this spectrum, was done on the basis of comparison with the calculated vibrational frequencies and infrared intensities for silylene (**6**) (Table 6), and with the known spectra of the hydroxysi-

Table 2
Vibrational frequencies for methyl(methoxy)silylene CH_3SiOCH_3 (**2**)

Mode	Frequencies (cm^{-1})			Assignment
	Calculated [a]	Observed		
		Ref. [24]	Present work	
1	18(0.2) [b]			CH_3(Si) twist
2	135(0.01)			CH_3(O) twist
3	167(4)			CSiOC out-of-plane bend
4	189(2)			CSiOC in-plane bend
5	321(9)			CSiOC out-of-plane bend
6	609(1)			HCSi rock
7	647(62)			Si–C str.
8	710(36)	709.2 w		HCSi rock; Si–O str. in-phase
9	805(64)	791.7 m		HCSi rock; Si–O str. out-of-phase
10	1098(226)	1084.3 vs	1084 m	C–O str
		1086.7 s		
		1106.5 m		
11	1179(0.5)			HCO rock
12	1200(34)	1218.8 m	1218 w	HCO rock
13	1265(33)		1262 w	HCSi deformation rock
14	1441(7)			CH_3(Si) deformation
15	1449(11)			CH_3(Si) deformation
16	1479(7)			CH_3(O) deformation
17	1491(2)			CH_3(O) deformation
18	1502(8)			CH_3(O) deformation
19	2995(72)	2842.2 w		CH_3(O) C–H symmetry str.
20	3002(5)			CH_3(Si) C–H symmetry str.
21	3067(40)			CH_3(O) C–H asymmetry str.
22	3068(11)			CH_3(Si) C–H asymmetry str.
23	3087(38)			CH_3(O) C–H asymmetry str.
24	3097(16)			CH_3(Si) C–H asymmetry str.

[a] B3LYP/6-311G(d,p).
[b] Calculated infrared intensities in km mol^{-1}.

Table 3
Vibrational frequencies for dimethylsilanone $(CH_3)_2Si{=}O$ (**3**)

Symmetry	Frequencies (cm^{-1})			Assignment
	Calculated [a]	Observed		
		Refs. [21–23]	Present work	
a_1	621(3) [b]			Si–C symmetry str.
b_2	686(10)	657 w		Si–C asymmetry str.
b_1	800(32)	770 m	771 m	CH_3 rock
b_2	810(128)	798 vs	799 s	CH_3 asymmetry rock
				Si–C asymmetry str.
a_1	863(22)	822 m	823 w	CH_3 symmetry in-plane rock
a_1	1227(99)	1210 vs	1210 s	Si=O str.
b_2	1290(36)	1240 m	1239 m	CH_3 asymmetry deformation rock
a_1	1296(48)	1244 m	1245 w	CH_3 symmetry deformation
b_1	1466(22)			CH_3 deformation

[a] B3LYP/6-311G(d,p).
[b] Calculated infrared intensities in km mol^{-1}.

lylene HSiOH [4,25] and dimethoxysilylene $(CH_3O)_2Si$ [24]. The absorptions of the Si–H stretch at 1925 cm^{-1} and of the C–O stretch at 1086 cm^{-1} (1074.1 cm^{-1} in $(CH_3O)_2Si$ [24]), provide particular support for the structural identification of **6**.

Only very weak bands of the $Si{\cdots}O(H)CH_3$ complex (**7**) and of the methyl(hydroxy)silylene (**8**) were observed in the spectrum (shown in Fig. 3(b)). The assign-

Table 4
Vibrational frequencies for 1-methyl-2-oxa-1-silirane (**4**)

Mode	Frequencies (cm^{-1})		Assignment
	Calculated [a]	Observed	
1	122(0) [b]		CH_3 torsion
2	212(1)		CSiC wag
3	232(10)		CSiC rock
4	568(1)		Si–H wag
5	626(16)		Si–H rock; HCSi rock out-of-plane
6	711(26)		Si–CH_3 str.; CH_2 rock
7	720(31)		Si–CH_2 str; HCSi rock
8	730(18)		Si–O str.; Si–H rock
9	822(81)	Overlapped by **3**	HCSi rock; Si–H wag
10	833(57)		CH_2 rock; HCSi rock
11	904(66)	935 vw	Si–H rock; HCSi rock
12	1020(95)	1006 w	C–O str.
13	1106(2)		CH_2 twist
14	1129(4)		CH_2 wag
15	1303(25)		CH_3 symmetry deformation
16	1456(6)		CH_3 asymmetry deformation
17	1459(6)		CH_3 asymmetry deformation
18	1475(2)		CH_2 scissor
19	2244(126)	2110 w	Si–H str.
20	3029(2)		CH_3 symmetry str.
21	3069(29)		CH_2 symmetry str.
22	3096(7)		CH_3 asymmetry str.
23	3117(5)		CH_3 asymmetry str.
24	3144(18		CH_2 asymmetry str.

[a] B3LYP/6-311G(d,p).
[b] Calculated infrared intensities in km mol^{-1}.

Table 5
Vibrational frequencies for 1-methoxy-1-silene $CH_3O(H)Si{=}CH_2$ (**5**)

Symmetry	Frequencies (cm^{-1})		Assignment
	Calculated [a]	Observed [24]	
a''	72(0.04) [b]		CH_3 torsion
a'	138(8)		COSi in-plane bend
a''	139(10)		COSi out-of-plane bend
a'	335(11)		OSi=C in-plane bend
a''	360(32)		Si–H out-of-plane bend; CH_2 out-of-plane bend; i.p. [c]
a''	581(12)	561.8 w	Si–H out-of-plane bend; C–H(CH_3) out-of-plane bend; i.p. [c]
a'	679(26)		Si–H in-plane rock; CH_2 in-plane rock; o.p. [c]
a''	705(43)	671.1 m	CH_2 wag; Si–H wag
a'	740(12)	752.1 w	Si–O str.
a'	885(112)	862.5 s	Si–H in-plane rock; CH_2 in-plane rock; i.p. [c]
a'	1022(45)	1002.5 m	Si=C str.
a'	1132(259)	1100.2 vs	C–O str.
a''	1175(1)		CH_3 rock
a'	1205(76)	1199.0 w	CH_3 in-plane rock
a'	1383(26)	1318.1 w	CH_2 scissor
a'	1488(3)		CH_3 symmetry deformation
a'	1498(8)	1462.3 w	CH_3 symmetry deformation
a''	1499(9)	1464.5 w	CH_3 asymmetry deformation
a'	2317(61)	2241.9 m	Si–H str.
a'	3010(53)		CH_3 symmetry str.
a''	3068(40)		CH_3 asymmetry str.
a'	3113(27)		CH_3 symmetry str.
a'	3144(0.1)		CH_2 symmetry str.
a'	3232(0.5)		CH_2 asymmetry str.

[a] B3LYP/6-311G(d,p).
[b] Calculated infrared intensities in km mol^{-1}.
[c] i.p., in phase; o.p., out of phase.

ment of these bands to the intermediates **7** and **8** was suggested after comparison with their calculated spectra, listed in Tables 7 and 8. These data indicate that this reaction (Scheme 2) proceeds spontaneously, and that the insertion of Si atoms into the O–H bond is preferred over insertion into the C–O bond.

Photolysis of the matrix with full light ($\lambda > 200$ nm) causes a complete disappearance of the bands of silylene (**6**) and of minor products **7** and **8**, and an emergence of a new peaks in the IR spectrum (Fig. 3(c)). The most intense new peaks, numbered in this spectrum, were assigned to methylsilanone (**9**) on the basis of comparison with the earlier observed single IR peak for matrix-isolated **9** [26] and with our calculations of the vibrational spectrum of **9** (Table 10). The weaker new peaks in the spectrum of the photolyzed matrix (Fig. 2(c)) were tentatively assigned to another structural isomer of silylene (**6**), 1-oxa-2-silirane (**10**), since their locations are in agreement with the calculated most intense IR features of **10** (Table 10). The new intense peak at 1104 cm^{-1}, which does not weaken during matrix warm-up experiments, while all peaks, attributed to products **9** and **10** have been depleted, was therefore assigned to a stable product-dimethoxysilane, $(CH_3O)_2SiH_2$ [27]. This product likely results from the insertion of silylene (**6**) into the O–H bond of methanol.

The simultaneous deposition and irradiation of the $Si/CH_3OH/Ar$ co-condensate resulted in a matrix, whose IR spectrum showed predominantly the bands of silanone (**9**) and only tiny absorptions from silirane (**10**). No bands of the products **6**–**8** were observed in these experiments, which presumably indicates that silanone (**9**) is the most photostable intermediate of the reaction (Scheme 2).

Table 6
Vibrational frequencies for methoxysilylene CH_3OSiH (**6**)

Symmetry	Frequencies (cm^{-1})		Assignment
	Calculated [a]	Observed	
a''	150(2) [b]		CH_3 torsion
a'	274(4)		COSi bend
a''	379(0.3)		Si–H twist
a'	742(34)	749 w	Si–O str.
a'	864(112)	859 m	Si–H in-plane rock
a'	1101(181)	1086 s	C–O str.
a''	1178(0.6)		CH_3 rock
a'	1202(25)		CH_3 rock
a'	1479(4)		CH_3 symmetry deformation
a''	1489(2)		CH_3 asymmetry deformation
a'	1500(11)		CH_3 symmetry deformation
a'	1995(375)	1925 s	Si–H str.
a'	2995(58)		CH_3 symmetry str.
a'	3072(35)		CH_3 symmetry str.
a''	3094(30)		CH_3 asymmetry str.

[a] B3LYP/6-311G(d,p).
[b] Calculated infrared intensities in km mol^{-1}.

Table 7
Vibrational frequencies for complex $CH_3(H)O\cdots Si$ (**7**)

Symmetry	Frequencies (cm^{-1})		Assignment
	Calculated [a]	Observed	
a''	120(4) [b]		CH_3 torsion
a'	239(1)		C–O···Si bend
a'	378(37)		Si···O str.
a''	397(133)		O–H out-of-plane rock
a'	921(41)	965 m	C–O str.
a'	1038(64)	1002 s	O–H in-plane rock; CH_3 in-plane rock
a''	1157(3)		CH_3 out-of-plane rock
a'	1300(3)		CH_3 in-plane rock; O–H in-plane rock
a'	1447(10)		CH_3 symmetry deformation
a''	1491(4)		CH_3 asymmetry deformation
a'	1492(9)		CH_3 symmetry deformation
a'	3033(71)		CH_3 symmetry str.
a''	3126(21)		CH_3 asymmetry str.
a'	3148(0.4)		CH_3 asymmetry str.
a'	3830(182)		O–H str.

[a] B3LYP/6-311G(d,p).
[b] Calculated infrared intensities in km mol^{-1}.

Table 8
Vibrational frequencies for methyl(hydroxy)silylene CH_3SiOH (**8**)

Symmetry	Frequencies (cm^{-1})		Assignment
	Calculated [a]	Observed	
a''	17(0.4) [b]		CH_3 torsion
a'	280(4)		CSiO bend
a''	521(47)		O–H out-of-plane rock
a'	643(63)		Si–C str.
a''	649(39)		HCSi rock; O–H rock
a'	753(47)	786	HCSi in-plane rock; O–H in-plane rock
a'	837(53)	831	Si–O str.
a'	883(196)	881	O–H in-plane rock
a'	1267(37)		CH_3 deformation rock
a'	1440(9)		CH_3 symmetry deformation
a''	1449(12)		CH_3 asymmetry deformation
a'	3001(4)		CH_3 symmetry str.
a''	3067(10)		CH_3 asymmetry str.
a'	3099(14)		CH_3 symmetry str.
a'	3860(95)		O–H str.

[a] B3LYP/6-311G(d,p).
[b] Calculated infrared intensities in km mol^{-1}.

Table 9
Vibrational frequencies for 1-oxa-2-silirane (**10**)

Mode	Frequencies (cm^{-1})		Assignment
	Calculated [a]	Observed	
a''	492(2) [b]		SiH_2 torsion
a'	607(2)		C–O str; SiH_2 wag
a''	643(36)		SiH_2 rock
a'	731(35)	729	Si–C str; Si–O str, asymmetry
a'	765(119)	763	SiH_2 wag; Si–C str
a''	822(40)	826	CH_2 rock; SiH_2 rock; i.p. [c]
a'	951(36)	942	SiH_2 scissor
a'	1032(97)	1024	C–O str, Si–O str symmetry; SiH_2 scissor
a''	1110(2)		CH_2 rock.
a'	1126(3)		CH_2 wag
a'	1475(2)		CH_2 scissor
a'	2257(61)		Si–H symmetry str.
a''	2273(128)		Si–H asymmetry str.
a'	3074(25)		C–H symmetry str.
a''	3152(16)		C–H asymmetry str.

[a] B3LYP/6-311G(d,p).
[b] Calculated infrared intensities in km mol^{-1}.
[c] i.p., in phase.

4. Discussion

4.1. Mechanistic consideration

The matrix isolation experiments have demonstrated that the reactions of Si atoms both with CH_3OCH_3 and CH_3OH proceed stepwise and involve a variety of reactive intermediates, such as complexes, silylenes, silenes, silanones and oxasiliranes, the IR identification of most of which has been suggested. In order to gain additional support for the structural characterization of these intermediates and for the reaction mechanisms,

Table 10
Vibrational frequencies for methylsilanone $CH_3(H)Si{=}O$ (**9**)

Symmetry	Frequencies (cm^{-1})			Assignment
	Calculated [a]	Observed		
		Ref. [26]	Present work	
a''	78(1) [b]			CH_3 torsion
a'	278(23)			CSiO rock
a''	492(21)			Si–H out-of-plane rock; HCSi rock
a'	658(2)			Si–C str.
a'	767(81)		756 s	HCSi in-plane rock; Si–H in-plane rock, out-of-phase
a''	776(37)			HCSi out-of-plane rock
a'	945(53)		929 m	HCSi in-plane rock; Si–H in-plane rock,
a'	1226(89)	1207.6	1208 s	Si=O str.
a'	1291(48)		1244 w	CH_3 symmetry deformation rock.
a'	1448(6)			CH_3 symmetry deformation
a''	1452(11)			CH_3 asymmetry deformation
a'	2215(140)		Overlapped by contaminant absorption at 2130–2230 cm^{-1} [5–8]	Si–H str.
a'	3023(0.3)			CH_3 symmetry str.
a''	3085(3)			CH_3 asymmetry str.
a'	3132(1)			CH_3 symmetry str.

[a] B3LYP/6-311G(d,p).
[b] Calculated infrared intensities in km mol^{-1}.

Table 11
Calculated B3LYP/6-311G(d,p) absolute energies (AE) and zero-point energies (ZPE) for the reactants, products and transition states

$Si(^1D)+CH_3OCH_3$	AE (hartrees)	ZPE (kcal mol^{-1})	$Ge(^1D)+CH_3OCH_3$	AE (hartrees)	ZPE (kcal mol^{-1})
$Si(^1D)$	−289.352428046		$Ge(^1D)$	−2076.88902132	
CH_3OCH_3	−155.071920086	49.75			
$(CH_3)_2O$–Si	−444.460098468	50.88	$(CH_3)_2O$–Ge	−2231.99158490	50.71
TS1	−444.420380917	48.00	TS1′	−2231.94515075	47.65
CH_3OSiCH_3	−444.605268573	48.63	CH_3OGeCH_3	−2232.10413783	48.09
TS2	−444.515447746	46.54	TS2′	−2231.99429927	45.84
$(CH_3)_2Si{=}O$	−444.641605855	47.85	$(CH_3)_2Ge{=}O$	−2232.09252190	46.99
TS3	−444.525845516	45.63	TS3′	−2232.00394121	44.40
$CH_2{=}Si(H)OCH_3$	−444.582908959	47.06	$CH_2{=}Ge(H)OCH_3$	−2232.04755459	45.94
TS4	−444.541020404	45.84	[a]		
$CH_3(H)\overline{SiOC}H_2$	−444.596740648	47.36	[a]		
$Si(^1D)+CH_3OH$			$Ge(^1D)+CH_3OH$		
CH_3OH	−115.757393658	32.06			
$CH_3(H)O$–Si	−405.148341553	33.08	$CH_3(H)O$–Ge	−2192.67949739	32.87
TS5	−405.132833218	28.90	TS5′	−2192.65917738	28.23
CH_3OsiH	−405.261315512	30.76	CH_3OGeH	−2192.76385868	29.99
TS6	−405.103553807	30.34	TS6′	−2192.62944845	30.09
CH_3SiOH	−405.296522157	31.12	CH_3GeOH	−2192.79593977	30.68
TS7	−405.171113592	28.50	TS7′	−2192.65444508	27.56
$CH_3(H)Si{=}O$	−405.296315654	29.83	$CH_3(H)Ge{=}O$	−2192.75167399	28.78
TS8	−405.206025030	27.58	[a]		
$H_2\overline{SiOC}H_2$	−405.252841147	29.32	[a]		
TS9	−405.202570631	27.20	TS9′	−2192.67527704	26.70
TS10	−405.218983470	28.05	TS10′	−2192.69767000	27.01
$CH_2{=}Si(H)OH$	−405.274830492	29.27	$CH_2{=}Ge(H)OH$	−2192.74006079	28.32

[a] The routes to germaoxiranes have not been considered by present modeling.

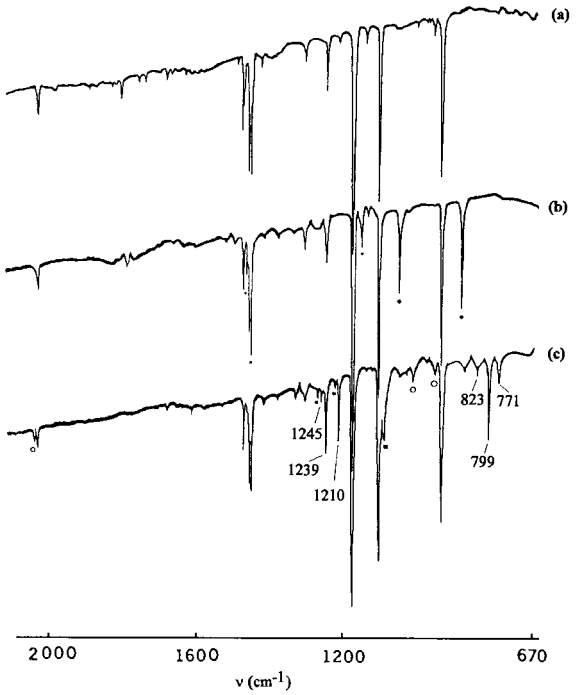

Fig. 1. FTIR spectra (15 K): (a) co-condensate of CH_3OCH_3 and Ar at molar ratio of 1:500; (b) co-condensate of Si atoms, CH_3OCH_3 and Ar at molar ratio of 1:1:500; (c) the same matrix after UV irradiation ($\lambda > 200$ nm). Labels: ●, complex Si···O(CH_3)$_2$; ■, silylene CH_3OSiCH_3; ○, 1-methyl-2-oxa-1-silirane; numbers, silanone $(CH_3)_2Si{=}O$.

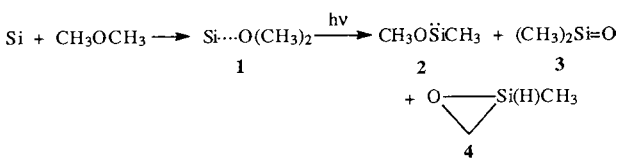

Scheme 1.

suggested in Schemes 1 and 2 on basis of experimental data, we have conducted the theoretical modeling studies, which are now discussed.

4.1.1. Theoretical modeling of the reactions of Si and Ge atoms with CH_3OCH_3

The schematic energy profiles of the studied reactions, drawn on the basis of the density functional B3LYP-6-311G(d,p) calculations performed for the singlet ground- and transition-state energies, are shown in Fig. 3. The reliability of the relative energy values, produced by this calculation method, follows from comparison of our B3LYP/6-311G(d,p) energy data for the Si(^{1}D) + H_2O reaction (calculated as a test) with the energies, calculated by the high level ab initio methods (MP4SDTQ//MP2 and CCSD//MP2), for the H_2SiO isomers [28], formed in this reaction; these data have demonstrated a remarkable agreement (within ± 1.0 kcal mol^{-1}).

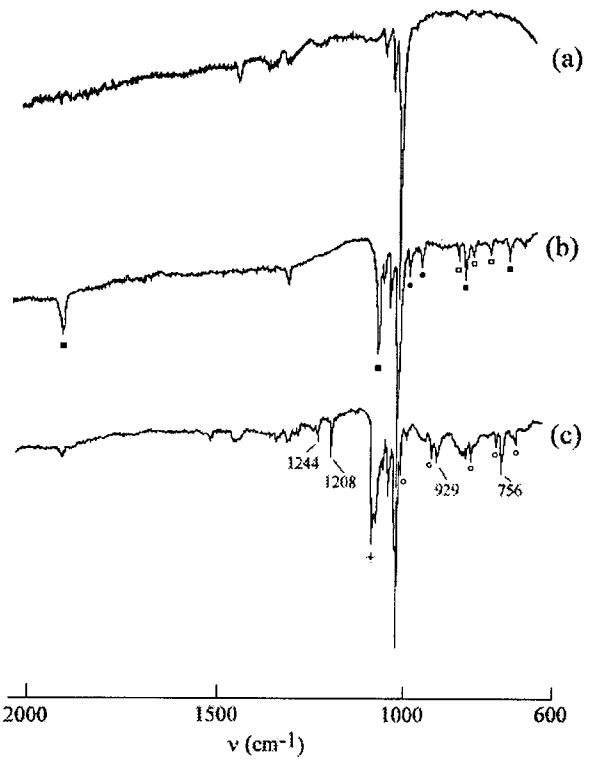

Fig. 2. FTIR spectra (15 K): (a) co-condensate of CH_3OH and Ar at molar ratio of 1:500; (b) co-condensate of Si-atoms, CH_3OH and Ar at molar ratio of 1:1:500; (c) the same matrix after UV irradiation ($\lambda > 200$ nm). Labels: ●, complex Si···O(CH_3)H; ■, CH_3OSiH; □, CH_3SiOH; ○, 1-oxa-2-silirane; +, $(CH_3O)_2SiH_2$. Numbers denote bands of silanone $CH_3(H)Si{=}O$.

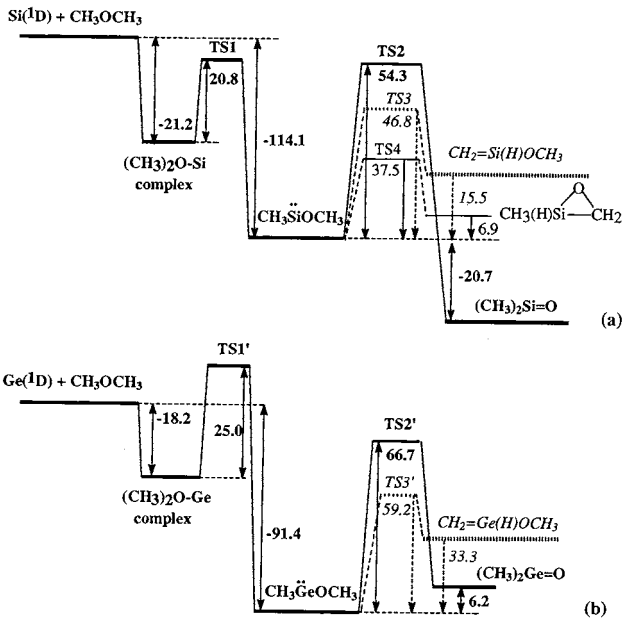

Fig. 3. Schematic energy profiles of the reactions of (a) Si(^{1}D) + CH_3OCH_3; and (b) Ge(^{1}D) + CH_3OCH_3. All energy values are corrected by ZPE.

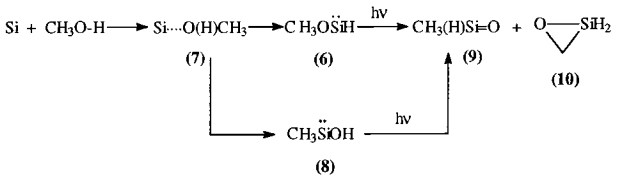

Scheme 2.

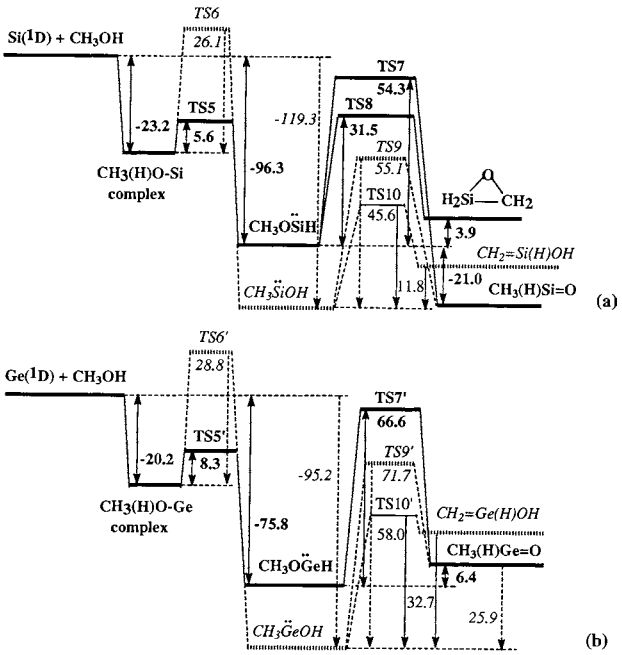

Fig. 4. Schematic energy profiles of the reactions of (a) $Si(^1D) + CH_3OH$, and (b) $Ge(^1D) + CH_3OH$. All energy values are corrected by ZPE.

Our calculations predict that formation of the $(CH_3)_2O\cdots Si$ complex (**1**) in the fist step of the $Si(^1D) + CH_3OCH_3$ reaction is exothermic by 21.2 kcal (Fig. 3(a)). The next step — insertion of Si into the C–O bond to yield methyl(methoxy)silylene **2** — is even more exothermic (114.1 kcal mol^{-1}). However, **1** is still separated from **2** by a barrier of 20.8 kcal mol^{-1}. This explains the observation of only complex **1** as the single product in the experiments performed without photoirradiation of the reaction co-condensate.

The isomerization of silylene (**2**) involving the CH_3 group migration results in dimethylsilanone (**3**), which is calculated to lie 20.7 kcal mol^{-1} lower in energy than **2**, which is separated from **3** by a high barrier of 54.3 kcal mol^{-1}. The other possible isomerization route for **2** implies the silylene-to-silene transformation into 1-methoxy-1-silene **5** via a 1,2 H shift. This route is calculated to be endothermic (15.5 kcal mol^{-1}) and proceeding through a barrier of 46.8 kcal mol^{-1}. The formation of silirane (**4**), which includes the intramolecular insertion into the C–H bond of the methoxy group in the singlet silylene (**2**), is less endothermic (6.9 kcal mol^{-1}) and has a lower barrier (37.5 kcal mol^{-1}).

The comparison of the calculated and experimentally observed transformation routes for the silylene (**2**) suggests that these passages are controlled mainly by thermodynamic rather than kinetic reasons, which likely account for the detection of the silanone (**3**) as a major product and the silirane (**4**) as a minor product and no observation of silene (**5**) in our experiments.

Based on these considerations and the comparison of calculated energy profiles (Fig. 3(a, b)), one can foresee that the similar photochemical reaction of Ge atoms with CH_3OCH_3 will be less selective towards the production of the dimethylgermanone (**11**) and be more reluctant to proceed. Germanone (**11**) is predicted to lie 6.2 kcal mol^{-1} higher in energy that its isomer, methyl(methoxy)germylene (**12**), and the barrier, separating **12** from **11**, is found to be 66.7 kcal mol^{-1} (Fig. 3(b)). The insertion of germanium into the C–O bond is also predicted to pass through a higher barrier (25 kcal mol^{-1}) than that of the silicon atom (Fig. 3(a)).

4.1.2. Theoretical modeling of the reactions of Si and Ge atoms with CH_3OH

The schematic energy profiles of these reactions, composed on the basis of DFT calculated relative energies of the products and transition states, are shown in Fig. 4. The formation of the $CH_3(H)O\cdots Si$ complex (**7**) (Scheme 2) in the first step of the $Si(^1D) + CH_3OH$ reaction is calculated to be exothermic by 23.2 kcal (Fig. 4(a)). The further insertions of Si atoms into either O–H or C–O bond of methanol are predicted to proceed with very different barriers (5.6 and 26.1 kcal mol^{-1}, respectively), and exothermicities (96.3 and 119.3 kcal mol^{-1}, respectively) to form the corresponding silylenes CH_3OSiH (**6**) and CH_3SiOH (**8**) (Fig. 4(a) and Scheme 2). These calculated data suggest a much easier insertion of silicon into the O–H bond than into the C–O linkage, in agreement with our observation of the spontaneous character of this reaction, which goes on in the absence of photoactivation, with predominant formation of silylene (**6**).

Among the further transformations of silylenes (**6**) and (**8**), only the isomerization of **6** into methylsilanone (**9**) has been predicted to be exothermic (21.0 kcal mol^{-1}), while the isomerization of **8** into the same product **9**, is almost thermoneutral, and the isomerization of **8** into 1-hydroxy-1-silene CH_2=Si(H)OH (**13**) and the intramolecular conversion of **6** into the silirane **10** are both endothermic (11.8 and 3.9 kcal mol^{-1}, respectively). Isomerizations of **6** and **8** into the same silanone **9** proceed over high but very similar barriers (54.3 and 55.1 kcal mol^{-1}, respectively), while for the transformations of **6** into **10** and of **8** into **13** overcoming of lower barriers is required (31.5 and 45.6 kcal mol^{-1}, respectively).

4.2. Molecular geometries of molecules **1**–**10**

The B3LYP/6-311G(d,p) optimized structures and geometry parameters for molecules **1**–**10** are given in Fig. 5. The calculations yielded structures with C_{2v} symmetry for complex **1** and silanone (**3**), C_1 symmetry for silylene (**2**) and silirane (**4**), and C_s symmetry for molecules **5**–**10**. The Si···O coordination bond distance in the complex **7** (1.970 Å) is calculated to be slightly shorter than that in **1** (1.985 Å), which is in line with the computed higher exothermicity of complexation of a Si atom with the CH_3OH molecule (23.2 kcal mol^{-1}) than with CH_3OCH_3 (21.2 kcal mol^{-1}). The Si–O bond lengths in the silylenes (**2**), (**6**), and (**8**) (1.673, 1.667, and 1.679 Å, respectively) and their valence angles at silicon (96.5, 94.3, and 96.8°, respectively) are found to track closely those in *trans*-HSiOH (1.668 Å, 94.8°), calculated recently using a costly coupled cluster method CCSD(T) and larger basis set (VQZ/VTZ) [29].

In the silanones (**3**) and (**9**), the DFT calculated Si=O bond distances are practically identical (1.530 Å), while the valence angles at Si atom slightly differ (111.8 and 110.7°, respectively). They are fairly close to the respective gas-phase geometry parameters of the parent silanone $H_2Si{=}O$ (1.515 Å and 112°), obtained by Bogey et al. [30]. The main geometrical parameters calculated by us for the silene (**5**), e.g. the Si=C bond length (1.697 Å) and valence angles at Si and C atoms (106.9 and 115.9°, respectively), compare adequately with those determined experimentally for the other simple silenes, $H_2Si{=}CH_2$ (1.704 Å, 115.2 and 116.0°) [31] and $(CH_3)_2Si{=}CH_2$ (1.692 Å, 111.4 and 114.2°) [32].

Our B3LYP/6-311G(d,p) calculations predict a highly strained geometry of the yet unknown silaoxiranes (**4**) and (**10**), in which the intracyclic OSiC angles (50.4 and 50.1°, respectively) are found to be close to the CSiC angle (49.2°) in the highly strained 1,1-dimethyl-1-siliranes [33]. In silaoxiranes **4** and **10**, the endocyclic Si–C bonds (1.818 Å) are shorter than those in the acyclic molecules **2**, **3**, **8**, **9** (1.861–1.908 Å), while the C–O bonds (1.494 and 1.488 Å, respectively) are somewhat longer than in **1**, **2**, **5**–**7** (1.420–1.459 Å), and the Si–O bond lengths (1.680 Å) remain virtually unchanged with respect to silylenes **2**, **6**, **8**.

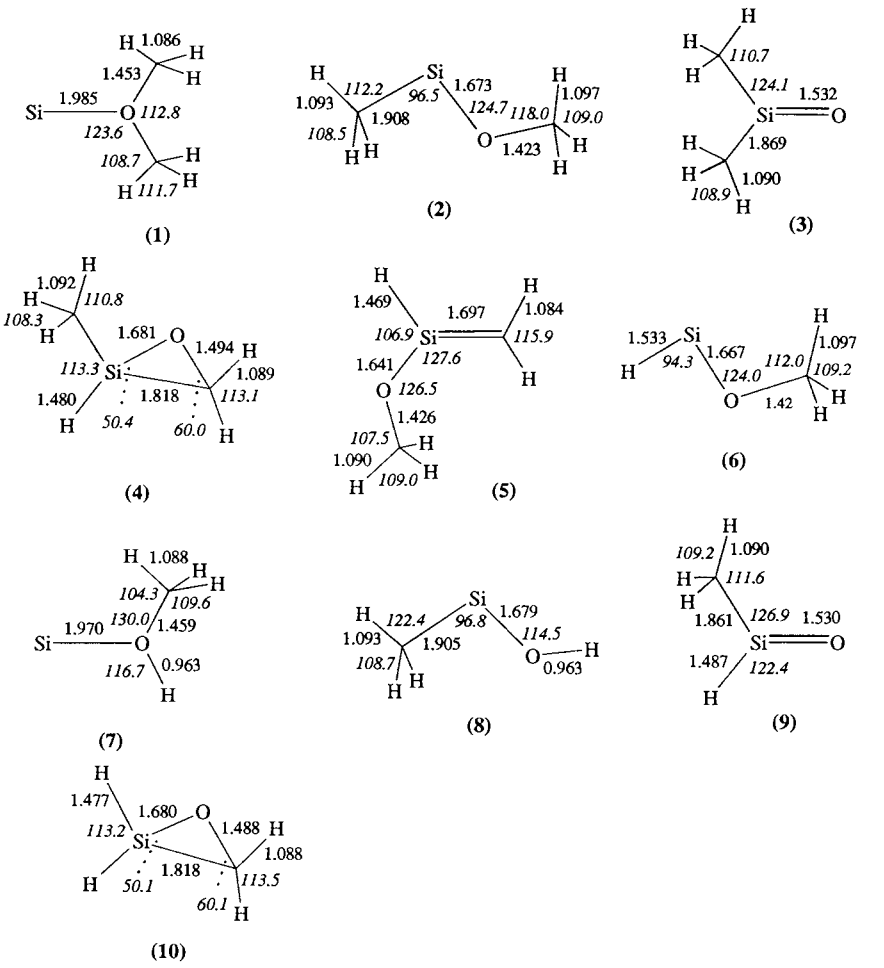

Fig. 5. B3LYP/6-311G(d,p) optimized geometries of **1**–**10**. Bond lengths (regular font) are given in Å, valence angles (italics) in degrees.

4.3. Vibrational analysis of the IR spectra of **1–10**

A full assignment of the observed IR bands, suggested with the aid of the DFT B3LYP/6-311G(d,p) calculations of harmonic frequencies and infrared intensities for molecules **1–10** and vibration animation, is given in Tables 1–10.

The most intense IR bands, observed for complexes **1** at 869, 1042 cm^{-1} (Table 1) and **7** at 965, 1002 cm^{-1} (Table 7), were assigned to the respective C–O symmetric and antisymmetric stretching vibrations and to the coupled in-plane OH and CH_3 rocking mode, in reasonable agreement with the calculations. The observed medium-intensity band at 1143 cm^{-1} and the two weak absorptions at 1456 and 1466 cm^{-1} in **1** were attributed to the CH_3 in-plane rock and corresponding CH_3 deformation modes. The bands of the stretching vibrations of the Si···O coordination bonds in **1** and **7** were not observed since they are predicted to lie below 450 cm^{-1}, beyond the detection range of the spectrometer used in our experiments.

In Table 2 the DFT calculated frequencies for the silylene CH_3SiOCH_3 (**2**) are compared with the experimental bands, earlier reported by Maier et al. [24] lacking vibrational assignment, and with those observed in the present work. Due to the lower yield of **2** obtained, we could detect only the three most intense bands of **2** in the 500–2000 cm^{-1} region, compared to five IR features revealed in Ref. [24]. The strongest band, observed at 1084.3 cm^{-1} (along with weaker satellites at 1086.7 and 1106 cm^{-1}) in Ref. [24] and at 1084 cm^{-1} by us, was attributed to the C–O stretching vibration, in agreement with the predicted high-intensity mode at 1098 cm^{-1} in **2**. The calculated frequency and intensity of the rocking vibration of the HCO moiety at 1200 cm^{-1} are consistent with the detected absorptions at 1218.8 cm^{-1} in Ref. [24] and 1218 cm^{-1} in the present work. The weak band detected by Maier et al. [24] (but not in the present work) at 709.2 cm^{-1} was assigned to the in-phase HCSi rocking mode coupled with the Si–O stretch, in accord with the calculated frequency of 710 cm^{-1} for this vibration (Table 2). On the basis of calculations and vibration animation, the bands at 791.7 and 2842.2 cm^{-1}, observed in Ref. [24], and not detected in our work presumably because of their overlap with the strong absorptions of the other products present in the matrix, were attributed to the out-of-phase HCSi rocking mode coupled with the Si–O stretch and to the C–H symmetric stretch of the CH_3O group, respectively. The assignment of a weak band at 1262 cm^{-1}, attributed in the present work to the silylene (**2**), to the HCSi deformation rocking mode is in accord with its predicted location at 1265 cm^{-1} (Table 2).

Among the spectral bands observed for the methoxysilylene (**6**), those at 749, 859 and 1086 cm^{-1} are in close agreement with the calculated frequencies at 742, 864 and 1101 cm^{-1} and intensities of the Si–O stretching, Si–H in-plane rocking and C–O stretching modes, respectively (Table 6). The suggested assignment of the band detected at 1925 cm^{-1} to the Si–H stretching mode in **6** is in reasonable accord with the DFT calculated frequency of this vibration at 1995 cm^{-1}. The three features detected at 786, 831, and 881 cm^{-1}, attributed in our experiments to the methyl(hydroxy)silylene (**8**), were tentatively assigned to the HCSi in-plane rocking, Si–O stretching and O–H in-plane rocking modes, respectively, based on their agreement with the computed frequencies at 753, 837 and 883 cm^{-1}.

The vibrational assignment for 1-methoxy-1-silene (**5**), in whose IR spectrum 11 bands have been observed by Maier et al. [24], is given in Table 5. The most intense feature reported at 1100.2 cm^{-1} is suggested to be the C–O stretching mode, in agreement with the predicted value of 1132 cm^{-1} and the calculated highest intensity of this vibration in **5**. To the CH_3 in-plane rocking mode, we attributed a band observed at 1199 cm^{-1}, which agrees with the calculated frequency of 1205 cm^{-1}. The observed medium intensity band at 1002.5 cm^{-1} is very likely to belong to the Si=C stretching mode, according to the DFT predicted value of 1022 cm^{-1}. The calculated frequency in **5** is shifted toward the higher wavenumbers relative to the predicted Si=C stretch in the parent silene $H_2Si{=}CH_2$, for which it was computed at 996 cm^{-1} [34] and observed at 985 cm^{-1} [35].

The high-intensity band reported in Ref. [24] at 862.5 cm^{-1} was assigned to the in-phase Si–H in-plane rocking mode coupled with the similar CH_2 in-plane mode in **5**, in agreement with the calculated value of 885 cm^{-1} and animation of this vibration. The assignment of a weak band at 752.1 cm^{-1} to the Si–O stretching mode is very likely, since this band is located in the IR region, typical for the Si–O single bond stretch in alkoxysilanes (e.g. $(CH_3)_3SiOCH_3$ [36]), and is close to the calculated value of 740 cm^{-1} for this motion in **5**. According to the calculations and vibration animation, a medium intensity band, observed at 671.1 cm^{-1} in Ref. [24], is attributed to the CH_2 wagging mode coupled with the SiH wagging mode.

Our DFT calculations predict the location of the CH_2 scissoring mode in **5** at 1383 cm^{-1}. The closest to this is the weak band, observed at as low as 1318.1 cm^{-1}. This large discrepancy can probably be explained only after independent spectral data for **5** are obtained. The two bands at 1462.3 and 1464.5 cm^{-1} are attributed to the symmetric and antisymmetric deformation modes of the CH_3 group, respectively, in agreement with the calculations. The observed band at 2241.9 cm^{-1} is located in the spectral region, characteristic for the $sp^2 = Si–H$ stretch [34,37]; therefore, the assignment to this mode in **5** seems to have no alternative.

The frequencies, experimentally established for dimethylsilanone (**3**) in Refs. [21–23] and observed in the present work, are compared in Table 3 with those, calculated in the 600–1500 cm^{-1} spectral region. Under the conditions of our experiments, we could observe five out of six bands, reported earlier for **3** [21–23]. The vibrational analysis of the full spectrum of dimethylsilanone (**3**), based on force field and DFT calculations, has already been published [22,23,38,39]; hence, it appeared unnecessary to discuss it here again.

As for the methylsilanone (**9**), in addition to the absorption, reported earlier by Withnall and Andrews [26], we were able to observe three more IR bands in the spectrum of this molecule (Table 10). Besides the strong band at 1208 cm^{-1} (discovered at 1207.6 cm^{-1} in Ref. [26]), which can be firmly assigned to the Si=O stretch, the other bands were found at 756, 929, and 1244 cm^{-1}. Based on DFT calculations of the spectrum of **9**, vibration animation and vibrational analyses, already performed for the other simple silanones [38,39], these features were attributed to the in-plane HCSi and SiH rocking modes, and symmetric CH_3 deformation rocking mode, respectively. We could not detect the predicted strong absorption band of the Si–H stretch, probably, because of its overlap with the prominent and broad contaminant absorption at 2130–2230 cm^{-1}, always present in the spectra of matrix trapped high-temperature silicon vapors in our apparatus [3,5–8].

Among the three weak IR bands attributed to 1-methyl-2-oxasilirane (**4**), one observed at 2110 cm^{-1} is of particular significance for the tentative identification of **4**, since it is located in the sp^3 Si–H stretch region. As expected, due to the electron withdrawing effect of oxygen, this vibration in **4** is red-shifted relative to that observed in the matrix-isolated 1-*tert*-butyl-2,2-dimethyl-1-silirane (2154 cm^{-1} [40]). Two other bands, observed at 935 and 1006 cm^{-1}, were assigned to the Si–H rocking and C–O stretching modes, respectively, in fair agreement with the calculated spectrum of **4** (Table 4).

For the parent oxasilirane (**10**), we have detected five IR bands in the 700–1050 cm^{-1} spectral region. They are compared with the calculated frequencies and infrared intensities for **10** in Table 9. Based on these calculations, the observed bands at 729, 763, 826, 942, and 1024 cm^{-1} were attributed to the coupled Si–C/Si–O stretch, SiH_2 wag, coupled in-phase CH_2/SiH_2 rock, SiH_2 scissors, and C–O stretch, respectively.

5. Conclusions

In the present work, we have directly observed the IR spectral features of several transient molecules, such as complexes $Si\cdots O(CH_3)_2$ (**1**) and $Si\cdots O(CH_3)H$ (**7**), silylenes CH_3OSiCH_3 (**2**), CH_3OSiH (**6**) and CH_3SiOH (**8**), silanones $(CH_3)_2Si{=}O$ (**3**) and $CH_3(H)Si{=}O$ (**9**), and 1-methyl-2-oxa-1-silirane (**4**) and oxasilirane (**10**), produced in the reactions of silicon atoms with dimethyl ether and methanol. The structural identification of molecules **2**, **3**, and **9**, based on the close match of their observed spectral fingerprints with those known from literature, has to be considered firm, whereas the assignment within the other transient species **1**, **4**, **6**–**8**, and **10**, is more tentative and rests mainly on mechanistic reasoning and comparison with the DFT calculations.

The observed formation of silanones in high yields in the reactions studied is particularly attractive, given both the fundamental interest in these Si=O π-bond-containing reactive intermediates and their important role in the microelectronics and materials technology as well as in combustion processes, surface and interstellar chemistries. For the purpose of direct spectroscopic characterization, the silanones have been previously generated by vacuum pyrolysis of silicon–oxygen-containing precursors [21–23,38,39], in situ oxidation of silanes [25,26] and dimethylsilylene [41], and insertion of SiO into ethane C_2H_6 [42], photoisomerization of alkoxysilylenes [24] in argon matrixes, and recently, by an electric discharge in the silane–oxygen–argon mixtures [30]. The photochemically induced cryogenic reactions of silicon atoms with molecules containing the C–O bond are studied in the present work using dimethyl ether and methanol. The results suggest new routes for generation and physical stabilization of transient silanones, and perhaps, for their heavier Group 14 (Ge, Sn, Pb) metallanone analogues.

Acknowledgements

This work has been supported at Rice by Mar Chem, Inc., The Robert A. Welch Foundation, a grant for supercomputer time from Houston Advanced Research Center, and in part by a US Army Research Office Grant No. DAAH04-96-1-0307 to Rice University.

References

[1] H.N. Waltenburg, J.T. Yates, Chem. Rev. 95 (1995) 1589.
[2] (a) A.V. Teplyakov, M.J. Kong, S.F. Bent, J. Chem. Phys. 108 (1998) 4599. (b) R. Konečný, D.J. Doren, Surf. Sci. 417 (1998) 169.
[3] (a) J.W. Kauffman, Ph.D. Thesis, Rice University, 1981. (b) J.W. Kauffman, R.H. Hauge, J.L. Margrave, in: J.L. Gole, W.C. Stwalley (Eds.), Metal Bonding and Interactions in High Temperature Systems, ACS Symposium Series, no. 179, 1982, p. 355.
[4] Z.K. Ismail, R.H. Hauge, L. Fredin, J.W. Kauffman, J.L. Margrave, J. Chem. Phys. 77 (1982) 1617.
[5] Z.K. Ismail, L. Fredin, R.H. Hauge, J.L. Margrave, J. Chem. Phys. 77 (1982) 1626.

[6] Z.H. Kafafi, R.H. Hauge, L. Fredin, J.L. Margrave, J. Phys. Chem. 87 (1983) 797.
[7] L. Fredin, R.H. Hauge, Z.H. Kafafi, J.L. Margrave, J. Chem. Phys. 82 (1985) 3542.
[8] Z. Xiao, Ph.D. Thesis, Rice University, Houston, 1991.
[9] G. Maier, A. Meudt, J. Jung, H. Pacl, Matrix isolation studies of silicon compounds, in: Z. Rappoport, Y. Apeloig (Eds.), The Chemistry of Organic Silicon Compounds, vol. 2, Wiley, New York, 1998, pp. 1143–1185.
[10] S. Sakai, M.S. Gordon, K.D. Jordan, J. Phys. Chem. 92 (1988) 7053.
[11] G. Jeong, K.J. Klabunde, J. Am. Chem. Soc. 108 (1986) 7103.
[12] V.N. Khabashesku, R.H. Hauge, J.L. Margrave, O.M. Nefedov, W.E. Billups, XXVIth Silicon Symposium, Indianapolis, IN, March 26–27, 1993, Abstract p. 39.
[13] S. Sakai, J. Deisz, M.S. Gordon, J. Phys. Chem. 93 (1989) 1888.
[14] (a) V.N. Khabashesku, O.M. Nefedov, International Conference on Low-Temperature Chemistry, September 5–9, 1994, Moscow, Russia, Abstract, p. 24. (b) V.N. Khabashesku, S.E. Boganov, K.N. Kudin, J.L. Margrave, J. Michl, O.M. Nefedov, Sixth International Conference on Chemistry of Carbenes and Related Intermediates, May 28–30, 1998, St. Petersburg, Russia, Proceedings, p. 22. (c) V.N. Khabashesku, K.N. Kudin, J.L. Margrave, J. Michl, S.E. Boganov, O.M. Nefedov, Russ. Chem. Bull. 48 (1999) 2003 (English); Izv. Akad. Nauk. Ser. Khim. (1999) 2027 (Russian).
[15] M.J. Frisch, G.W. Trucks, H.B. Schlegel, P.M.W. Gill, B.G. Johnson, M.A. Robb, J.R. Cheeseman, T.A. Keith, G.A. Petterson, J.A. Montgomery, K. Raghavachari, M.A. Al-Laham, V.G. Zakrzewski, J.V. Ortiz, J.B. Foresman, J. Cioslowski, B.B. Stefanov, A. Nanayakkara, M. Challacombe, C.Y. Peng, P.Y. Ayala, W. Chen, M.W. Wong, J.L. Andres, E.S. Replogle, R. Gomperts, R.L. Martin, D.J. Fox, J.S. Binkley, D.J. Defrees, J. Baker, J.P. Stewart, M. Head-Gordon, C. Gonzalez, J.A. Pople, GAUSSIAN 94, Gaussian, Inc., Pittsburg, PA, 1995.
[16] J.M. Seminario, P. Politzer (Eds.), Modern Density Functional Theory: A Tool for Chemistry, Elsevier, Amsterdam, 1995.
[17] (a) A.D. Becke, J. Chem. Phys. 98 (1993) 5648. (b) C. Lee, W. Yang, R.G. Parr, Phys. Rev. B 37 (1988) 785.
[18] (a) R. Krishnan, J.S. Binkley, J.A. Pople, J. Chem. Phys. 72 (1980) 650. (b) A.D. McLean, G.S. Chandler, J. Chem. Phys. 72 (1980) 5639. (c) M.J. Frisch, J.A. Pople, J.S. Binkley, J. Chem. Phys. 80 (1984) 3265.
[19] XMOL. Version 1.3.1. Minnesota Supercomputer Center, Inc., Minneapolis, MN, 1993.
[20] K.N. Kudin, J.L. Margrave, V.N. Khabashesku, J. Phys. Chem. 102 (1998) 744.
[21] (a) V.N. Khabashesku, Z.A. Kerzina, A.K. Maltsev, O.M. Nefedov, Izv. Akad. Nauk SSSR. Ser. Khim. (1986) 1215 (in Russian). (b) V.N. Khabashesku, Z.A. Kerzina, A.K. Maltsev, O.M. Nefedov, Bull. Acad. Sci. USSR. Div. Chem. (1986) 1108 (in English).
[22] A.K. Maltsev, V.N. Khabashesku, O.M. Nefedov, Low-temperature stabilization and direct spectroscopic study of intermediates with the Si=O multiple bonds, in: E.R. Corey, J.Y. Corey, P.P. Gaspar (Eds.), Silicon Chemistry, Ellis Horwood, Chichester, 1988, pp. 211–227, Chapter 21.
[23] V.N. Khabashesku, Z.A. Kerzina, A.K. Maltsev, O.M. Nefedov, J. Organomet. Chem. 347 (1988) 277.
[24] G. Maier, H.P. Reisenauer, K. Schöttler, U. Wessolek-Kraus, J. Organomet. Chem. 366 (1989) 25.
[25] (a) R. Withnall, L. Andrews, J. Am. Chem. Soc. 107 (1985) 2567. (b) R. Withnall, L. Andrews, J. Phys. Chem. 89 (1985) 3261.
[26] (a) R. Withnall, L. Andrews, J. Am. Chem. Soc. 108 (1986) 8118. (b) R. Withnall, L. Andrews, J. Phys. Chem. 92 (1988) 594.
[27] (a) D. Lin-Vien, N.B. Colthup, W.G. Fateley, J.G. Grasselli, The Handbook of Infrared and Raman Characteristic Frequencies of Organic Molecules, Academic, San Diego, CA, 1991. (b) L. Bellamy, The Infrared Spectra of Complex Molecules, third ed., vol. 1, Wiley, New York, 1975, p. 374.
[28] J. Kapp, M. Remko, P.v.R. Schleyer, J. Am. Chem. Soc. 118 (1996) 5745.
[29] J.M.L. Martin, J. Phys. Chem. A 102 (1998) 134.
[30] M. Bogey, B. Delcroix, A. Walters, J.C. Guillemin, J. Mol. Spectrosc. 175 (1996) 421.
[31] S. Bailleux, M. Bogey, J. Demaison, H. Bürger, M. Senzlober, J. Breidung, W. Thiel, R. Faigar, J. Pola, J. Chem. Phys. 106 (1997) 10016.
[32] H.S. Gutowsky, J. Chen, P.J. Hajduk, J.D. Keen, C. Chuang, T. Emilsson, J. Am. Chem. Soc. 113 (1991) 4747.
[33] G.L. Delker, Y. Wang, G.D. Stucky, R.L. Lambert, C.K. Haas, D. Seyferth, J. Am. Chem. Soc. 98 (1976) 1779.
[34] V.N. Khabashesku, K.N. Kudin, J.L. Margrave, J. Mol. Struct. 443 (1998) 175.
[35] C.A. Arrington, K.A. Klingensmith, R. West, J. Michl, J. Am. Chem. Soc. 106 (1984) 525.
[36] I.F. Kovalev, L.A. Ozolin, V.A. Arbuzov, I.V. Shevchenko, M.G. Voronkov, E.Ya. Lukevic, Izv. Akad. Nauk. Latv. SSSR (1970) 533.
[37] (a) G. Maier, G. Mihm, H.P. Reisenauer, Angew. Chem. Int. Ed. Engl. 20 (1981) 597. (b) H.P. Reisenauer, G. Mihm, G. Maier, Angew. Chem. Int. Ed. Engl. 21 (1982) 854. (c) G. Maier, G. Mihm, H.P. Reisenauer, Chem. Ber. 117 (1984) 2369.
[38] V.N. Khabashesku, Doctor of Sciences (Full Professor) Thesis, Zelinsky Institue of Organic Chemistry, Russian Academy of Science, Moscow, 1998.
[39] V.N. Khabashesku, Z.A. Kerzina, K.N. Kudin, O.M. Nefedov, J. Organomet. Chem. 566 (1998) 45.
[40] K.M. Welch, J. Michl, R. West, J. Am. Chem. Soc. 110 (1988) 6689.
[41] C.A. Arrington, R. West, J. Michl, J. Am. Chem. Soc. 105 (1983) 6176.
[42] M.J. Almond, Second International Conference on Low Temperature Chemistry, August 4–9, 1996, Kansas City, MO, Proceedings, pp. 112–117.